Simultaneous fluorescence and shadow imaging for wetting analysis

SIMULTANEOUS FLUORESCENCE AND SHADOW IMAGING FOR WETTING ANALYSIS

T. Hagemeier[1,c], K. Zähringer[1], D. Thévenin[1]

[1]Lab of Fluid Dynamics & Technical Flow, University of Magdeburg, 39106 Magdeburg, Germany
[c]Corresponding author: Tel.: +493916752097; Fax: +493916742840 ; Email: Thomas.hagemeier@ovgu.de

KEYWORDS:
Main subjects: surface film flow, wetting behavior
Fluid: droplet on horizontal and inclined plates
Visualization method(s): Laser Induced Fluorescence, Shadowgraphy
Other keywords: apparent contact angle, retention force

ABSTRACT: *Simultaneous fluorescence and shadow imaging is applied to investigate static droplets on an inclined plate. The first objective of this study is to elucidate whether fluorescence imaging is applicable for apparent contact angle measurements, particularly for configurations with large contact angles (>90°). The results showed large effect of the liquid surface curvature on the fluorescence signal even at smaller apparent contact angles. Additional measurements are required to enable a correction of this effect.*
The second objective of this study is to evaluate the retention force of droplets on an inclined plate. Here we used the length of perimeter segments (contact line segments) and corresponding apparent contact angles for an estimation. Eventually, we found a new retention force factor that yields better agreement between retention force and gravitational force in static conditions than others do.

1 Introduction

Liquid films on soft and solid surfaces attract interest from different research areas, e.g. for designing self-cleaning textiles or ceramics, manufacturing intelligent structures of packed columns, or for controlling exterior water flow on vehicles. In all scenarios, the typical liquid film morphology is a rivulet. Rivulets are subject to surface forces. Wetting properties, depending on the specific solid-liquid combinations, control their flow path. However, the understanding of wetting processes is incomplete. Various measurement principles exist to determine wetting parameters like surface tension, apparent contact angles, or free surface energies. Unfortunately, there is no comprehensive approach providing these details together with additional film flow parameters in complex situations. Local details usually get lost, when observing a larger region of interest (ROI). Fluorescence imaging is a method that allows capturing film flow parameters (like thickness and film propagation or contact line velocity) for larger ROI compared to local observations made with shadowgraphy for apparent contact angles. Therefore, fluorescence imaging has been applied very often to study liquid films, but mainly without considering wetting aspects. However, the fluorescence signal might contain even more information.
The objective of the work described in this paper is to find out which analysis of the fluorescence signal could deliver information concerning apparent contact angles. In particular, this study focusses on situations with apparent contact angles near 90° (as already described in Hagemeier et al. [1]) and above. A correction of the fluorescence signal to compensate for ambiguities associated with apparent contact angles larger 90° would highly facilitate liquid film experiments on plane surfaces. Fluorescence imaging would then provide film thickness, propagation and apparent contact angles simultaneously.

In this study, simultaneous fluorescence and shadowgraphy measurements serve as a basis and provide data for comparison. Even if 3D droplet shape analysis using shadowgraphy has already been reported in the past, e.g. [4], [5], fluorescence imaging has not been considered for contact angle analysis when apparent contact angles are above 90°. It is assumed that not only the fluorescence signal gradient close to the contact line but also the distance of the edge towards the nearest local maximum in film thickness have to be considered when analyzing apparent contact angles by fluorescence imaging.

1.1 Background on single droplet wetting

Characterizing the wetting behavior is essential for various industrial applications and attracted research interest from many sides, see for example [2], [11], [18], [19], [25]. A fundamental introduction towards surface wetting and associated contact angle investigations is given by Decker et al. [9], Kwok and Neumann [14], or more recently by Snoeijer and Andreotti [23]. The focus of our research is on single droplets deposited on horizontal plates. Plates we use are typically made of different materials and, therefore, show different surface energy or wetting properties. The materials of interest are acrylic glass, glass, and painted metal, as found typically in automobile application. Hence, this is a continuation of our work dealing with vehicle soiling investigations [26]. Researchers from the automotive industry still spend large effort to develop macroscopic liquid film models. However, important details are missing or not completely understood, as for instance the transition from static to dynamic droplets on walls or the coalescence and break-up behavior of droplets and rivulets. In general, droplets are displaced by gravitational force, shear stress, temperature gradients, concentration gradients of chemical components and electrostatic forces. However, we limit our investigation to droplets being displaced by gravity, when the initially horizontal plate is tilted by a specified angle. At the same time, the capillary force acts as a retention force and hinders the displacement. Tilted plate experiments reveal minimum and maximum contact angles, as well as the angle at which a droplet starts to move [8], [19]. Consequently, they are appropriate to estimate the wetting properties of different solid-liquid combinations.

Based on the Macdougall-Ockrent-Frenkel formula [12], [17]

$$\Delta\left(\cos\theta\right)_{r,a} = \frac{\rho g}{\gamma}\frac{V}{d}\sin\left(\alpha\right), \tag{1}$$

which is a force balance between the gravitational force and the capillary force, information concerning the mobility of the droplets can be derived. The variables are $\Delta(\cos\theta)_{r,a}$, which represents the change of cosine of the contact angle along the perimeter. Usually, this is simplified to the difference between advancing and receding contact angle. As usual, ρ is the fluid density, g is the constant of gravitational acceleration, γ is the surface tension, V is the liquid volume, d is a characteristic length of the droplet and α is the plate inclination. Usually, d is the sphere diameter corresponding to the volume V.

Besides proper experimental setups, Rio et al. [21] discussed the impact of spatial resolution. At macroscopic level, the aforementioned force balance of capillary force and gravity dictates the shape of a motionless droplet. Due to the discrepancy between observation and fluid dynamic theory, which leads to an infinite pressure at the contact line, contact line motion is often related to effects at molecular level (molecular forces, slip length). Rio et al. macroscopically investigated the properties of a moving contact line (angle and velocity). Furthermore, they used particle tracking to obtain the surface velocity vectors, which were found to be perpendicular to the contact line. This information leads to the conclusion that the dynamic contact angle is only a function of the local capillary number Ca that relates viscous forces to surface tension. The Ca number:

$$Ca = \frac{u\mu}{\gamma}, \tag{2}$$

relates u, the local contact line velocity, the fluid dynamic viscosity μ and the surface tension γ. However, in many cases, the capillary number is unknown due to missing information about the contact line (exact position and velocity). Instead, an effective capillary number is commonly used.
This effective capillary number includes the droplet velocity [24]. Le Grand et al. [15] considered the shape transition of droplets in their experiments. They investigated sliding droplets at different inclination angles. They reported four different droplet shapes, which vary with increasing capillary number from oval, to corner, to cusp and finally to pearling shape (break-up and deposition of smaller droplets). While the droplet shape significantly changes in width and length, it remains at a constant maximum height level for all four regimes. Moreover, they reported that a corner appears at the rear of the droplets for receding contact angles approaching a critical value larger than zero.
In this paper, we also report our effort on estimating the capillary force in more detail. Particularly, we measured the contact angle along the perimeter of the droplet together with the arc length of the contact line. This combination allows the explicit calculation of the capillary force F_c.

$$F_C = \sum_i l_{ch,i} \gamma \cos\theta_{app,i} \cos\varphi_i \tag{3}$$

In equation (3), i is the number of circle segments to describe the droplet contact line. An arc length $l_{ch,i}$, or an apparent contact angle $\theta_{app,i}$ corresponding to a specific azimuthal angle φ_i. Eventually, the cosine of the azimuthal angle describes the force component acting in stream-wise direction, when the plate is inclined. Comparing equations (1) and (3), differences occur in the characteristic length as well as in the contact angle. The differences are small or may even disappear for symmetrical droplets, e.g droplets at rest on a horizontal plate. However, these differences become significantly larger for increased inclination angles, which are associated with larger droplet deformation and asymmetry.

2 Experimental methodology

2.1 Hardware setup, operating parameters and calibration

The experimental setup combines both, fluorescence and shadow imaging techniques (as shown in Figure 1). The synchronized systems use individual illumination devices (LEDs) and CCD-cameras. Geometrical calibration provided scale factors of 0.0122 mm/pixel and 0.0137 mm/pixel for shadow and fluorescence imaging, respectively. Both techniques are used to quantify the liquid film thickness. Its gradient near the contact line corresponds to the apparent contact angle. For solid-liquid combinations with a static apparent contact angle well below 90°, it is possible to use the fluorescence signal for apparent contact angle measurement as well. This is beneficial when analyzing situations with droplets sliding down an inclined surface, or for rivulet flows. These scenarios generally involve larger ROIs as the droplets/rivulets propagate. Fluorescence imaging provides reasonable resolution of the liquid film thickness when the fluorescent dye tracer concentration and illumination intensity are set correctly. In our experiments, Resorufin is the fluorescent dye tracer and has a concentration of 50 mg/l in water. The illumination of the fluorescent mixture occurred by an array of green LEDs which were arranged to illuminate the liquid from the top (same direction as the camera observes the liquid). They show a center wavelength of 535 nm, while the excitation time is 8 ms. The cameras and LEDs operated at 5 frames per second, ensuring constant light energy output and extinction. Further camera settings are as follows for the fluorescence imaging: CCD camera of type Imager LX, 60 mm objective

lens at f-number 8, exposure time 8 ms and 535 nm high pass filter. The shadow imaging settings are: CCD camera type Imager LX, 60 mm objective lens at f-number 11, exposure time 20 µs and no additional filter.
The liquid-solid combination in our experiments involves the aforementioned fluorescent mixture and a smooth painted metal plate as solid substrate. This combination shows apparent static contact angles around 74°. This value is quite constant for droplet volumes of 30 µl and 50 µl. Generally, we dispense a droplet using a syringe-pump and place it on the initially horizontal metal plate. Then, two different procedures occurred depending on the corresponding objective.
Primary objective is the investigation of the retention force. Here, once a droplet was generated, we set the plate to a certain inclination angle, assuring that the droplet did not move. 0° to 40° plate inclination was feasible for 30 µl droplets, while static 50 µl droplets could be observed only until 30°. Then, the shadow camera rotated for 90° around the droplet, while acquiring images every 15°. This provides droplet profiles and contact angle data along the perimeter, as function of the azimuthal angle respectively.

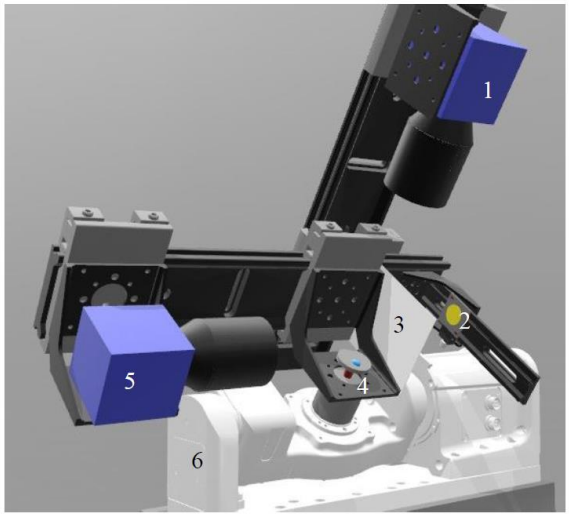

1 Fluorescence imaging camera

2 LED array

3 Screen

4 Droplet

5 Shadow imaging camera

6 Rotation and tilt device

Fig. 1. Experimental setup showing shadow imaging system (camera and background illumination by LED) aligned horizontally and fluorescence-imaging camera (shown without additional LED, arranged vertically), both mounted onto a rotation and tilt device to achieve various droplet shapes.

Additionally, we acquired top-view fluorescence images of the droplet. They contain information for the droplet perimeter and, more importantly, reveal the exact length of contact line segments.
Our second objective is the investigation of fluorescence imaging uncertainty, particularly associated to the curved shape of droplets and rivulets. Here, once the droplet is produced, we start the synchronized image acquisition while tilting the plate simultaneously. The inclination angle increases from 0° to around 55°, which is the critical angle for the droplets to start sliding down the plate. Accordingly, we obtain droplet profiles and fluorescence intensity for various droplet deformations. This data includes both, droplet shape parameters and fluorescence intensity required to assess the measurement quality. Figure 2 shows a typical pair of images acquired during the measurement.

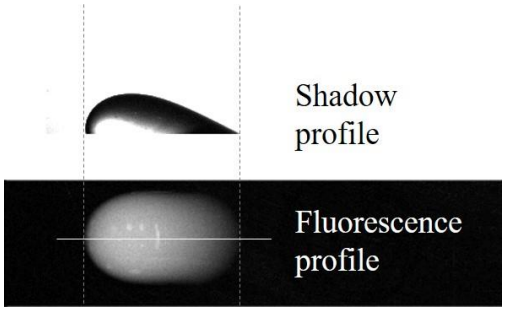

Fig. 2. Image pair coming from shadow camera (top) and fluorescence camera (bottom). The white horizontal line represents the fluorescence profile used during calibration process.

In order to account for any variation and random error, we repeated each test 5 times. A careful cleaning procedure after each try ensures independent measurement results.

However, the fluorescence imaging also requires calibration. Based on the Beer-Lambert law, the emitted fluorescence light intensity is proportional to the film thickness, when all other parameters (molar absorption coefficient, fluorescent dye tracer concentration, extinction light intensity) are constant. Usually, an integral evaluation of fluorescence intensities in an image of a single droplet of known volume allows assigning each film thickness value to a certain fluorescence intensity [3]. However, this procedure is hindered by the inaccuracy of the dosing system.

Therefore, we used the shadow images and corresponding height values to correlate with the fluorescence intensity. For this purpose, we correlate the shadow profile with the fluorescence intensity values along the center profile of the droplets top view (see Figure 2). This way, we can also investigate the influence of different surface shapes on the calibration outcome. The left plot of Figure 3 shows a typical calibration function where each pixel intensity value is assigned to a film thickness value. This function corresponds to the fluorescence signal obtained from a symmetric droplet at rest on a horizontal plate. We describe the fluorescence intensity in counts, which is similar to gray level or arbitrary unit. The linear shape of the calibration curve reveals a reliable conversion of intensity values into thickness values. Here, the calibration factor is cf = 0.0041 mm/count. Still, we observe a slight scattering around a mean value. We assess the quality of the linear fit in terms of r^2 value, here r^2=0.979, with r^2=1 being a perfect fit.

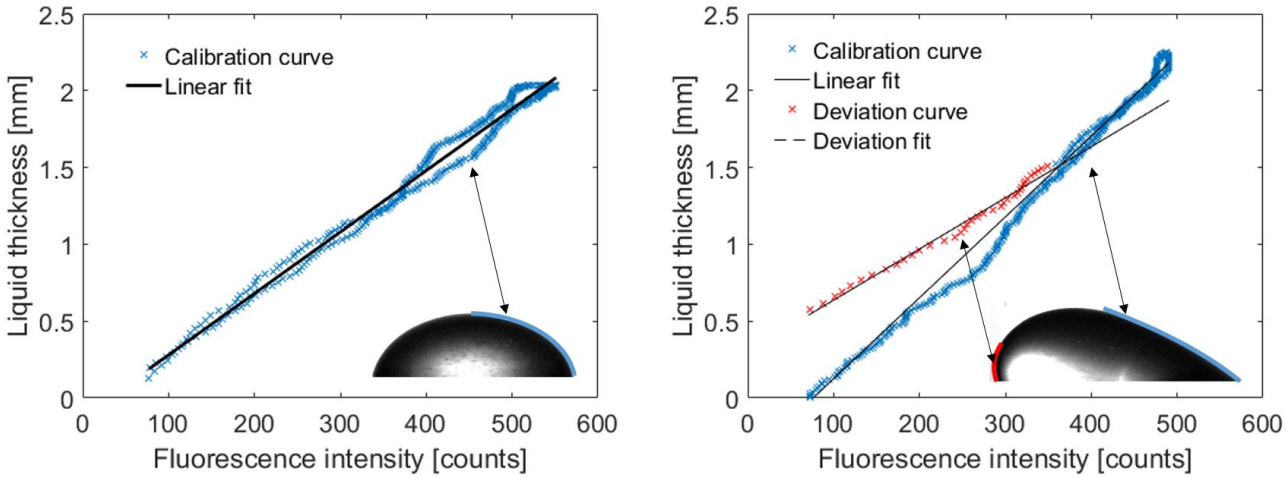

Fig. 3. Typical calibration function to convert fluorescence intensity values into film thickness values (left) and calibration function with ambiguity for contact angles above 90° (right). Corresponding shadow images are shown in the lower right corner of each plot.

In case of large contact angles, an ambiguity appears where one fluorescence intensity value corresponds to two thickness values, one on our calibration curve (the curve we assumed to be the calibration curve), and the other on a deviation curve (red curve in right plot of Figure 3). This leads not only to an ambiguity, but also to a change of the calibration curve parameters. This problem is discussed in section 3.2, where we analyze how the fluorescence signal changes with the shape of the object under investigation.

3 Results and discussion

3.1 Experimental results for retention force

One objective of this study was to measure the apparent contact angle and estimate corresponding curve lengths of the contact line. We obtained the apparent contact angles from shadow images, while the curve length, which is the length of 15° perimeter segments, is visible in the top view (fluorescence images).

Figures 3 and 4 present the evolution of the contact line with increasing inclination angle, for 30 and 50 µl droplets respectively.

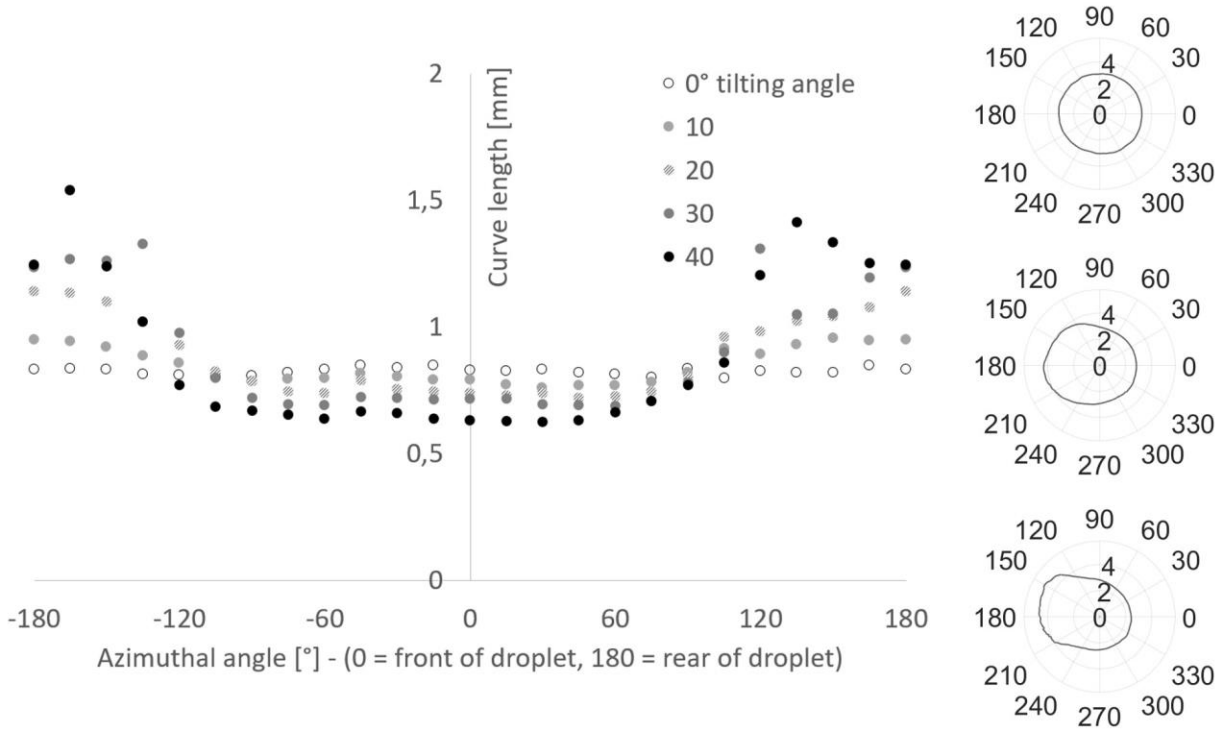

Fig. 4. Evolution of characteristic length (segments of contact line) as function of azimuthal angle for a 30 µl droplet sitting on an inclined plate at different tilting angles (plot on left side) and exemplary contact lines at 0°, 20° and 40° from top to bottom (polar plots on right side features radius given in mm with 0° equal to droplet front)

The data in both figures provides information about the length of contact line segments. Each data point corresponds to a segment of 15 degree of the circumference. The center point for this analysis, corresponding to the center of mass obtained as peak value in the fluorescence images, also changes

with increased plate inclination. Obviously, the droplet front steadily narrows and the local radius reduces, as can be seen in the polar plots. Simultaneously, the rear widens with increasing tilting angle. This leads to a significant asymmetry with respect to the wetted area.

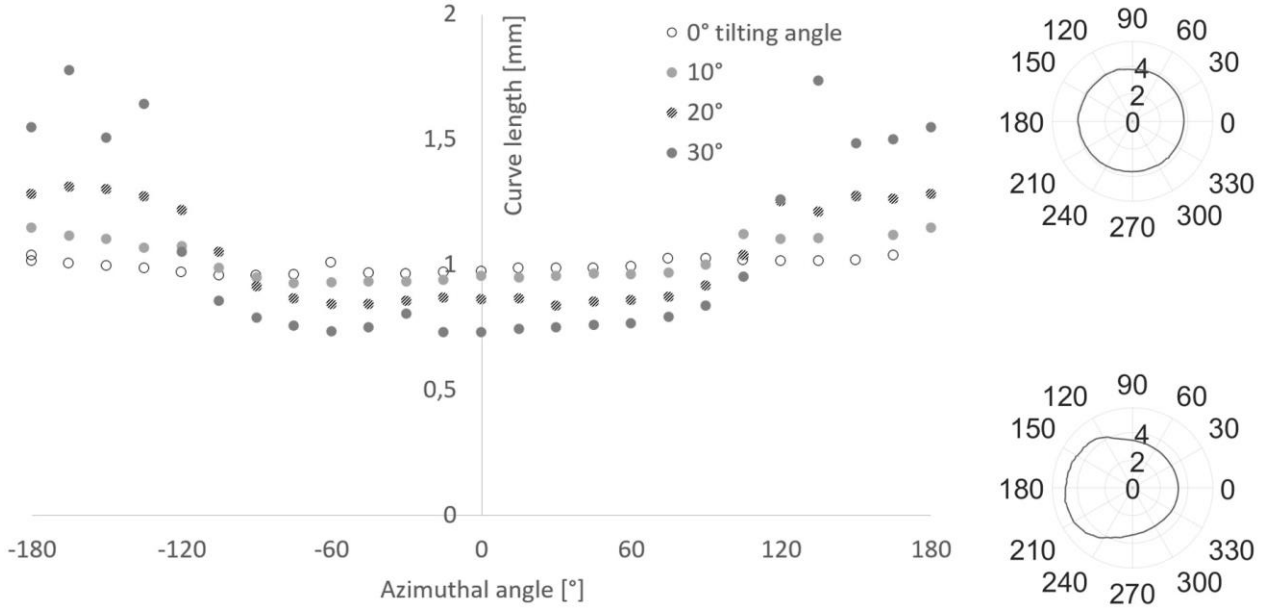

Fig. 5. Evolution of characteristic length (segments of contact line) as function of azimuthal angle for a 50 µl droplet sitting on an inclined plate at different tilting angles (plot on left side) and exemplary contact lines at 0° and 20° from top to bottom (polar plots on right side features the radius given in mm)

More values that are characteristic for the morphological changes, including total contact line length and wetted area are listed in Table 1. Besides geometrical values, the Bond number Bo shows up as well. It is the most important dimensionless number that relates gravitational force and surface tension force. The Bo number reads as:

$$Bo = \frac{\rho d^2 g \sin(\alpha)}{\gamma} \tag{4}$$

Characteristics	30 µl droplet			50 µl droplet		
Tilting angle [°]	Contact line length [mm]	Wetted area [mm²]	Bo number	Contact line length [mm]	Wetted area [mm²]	Bo number
0	19.79	31.07	0	23.82	44.86	0
10	20.26	32.38	0.35	24.59	47.07	0.49
20	21.01	34.35	0.69	24.73	47.42	0.97
30	21.63	34.52	1.01	25.25	46.05	1.42
40	21.14	32.51	1.3	-	-	

Table 1: Characteristic values for droplets at different plate inclination angles

In combination, we can calculate the capillary force or retention force according to equation (3). Figure 6 shows the resulting retention force as function of the gravitational force. In principle, the retention

force should be equal to the gravitational force for a static droplet in equilibrium state. Obviously, our method systematically overestimates the retention force. In order to evaluate this deviation, we processed the data in a different way using the functional relation of equation (1). Here, the retention force is calculated using the half-droplet length, similar to [8].
However, this method underestimates the retention force and it is always below the gravitational force. We know about the discrepancy between both forces, e.g. from the work of ElSherbini and Jacobi [27]. They report different retentive force factors k. These factors practically weigh the length in the capillary force to match it with the gravitational force (see equation (5)).

$$F_C = k\left(\cos\theta_R - \cos\theta_A\right)\gamma R \tag{5}$$

This factor varies for different studies summarized in [27] from a minimum value k=1 up to a maximum value equal to k=π. The questions is how to weigh our data, as we sum up individual parts with their own length and contact angle values to obtain the retention force. Eventually, summing capillary force contributions only for half of the wetted perimeter plus the advancing front and the receding back yields the best fit. Trying to express this in terms of a retentive force factor, we divide the perimeter length by the length that was used to calculate the capillary force (half perimeter plus advancing front and receding back lengths). This procedure yields a single value of k=1.84 for all of our experiments.

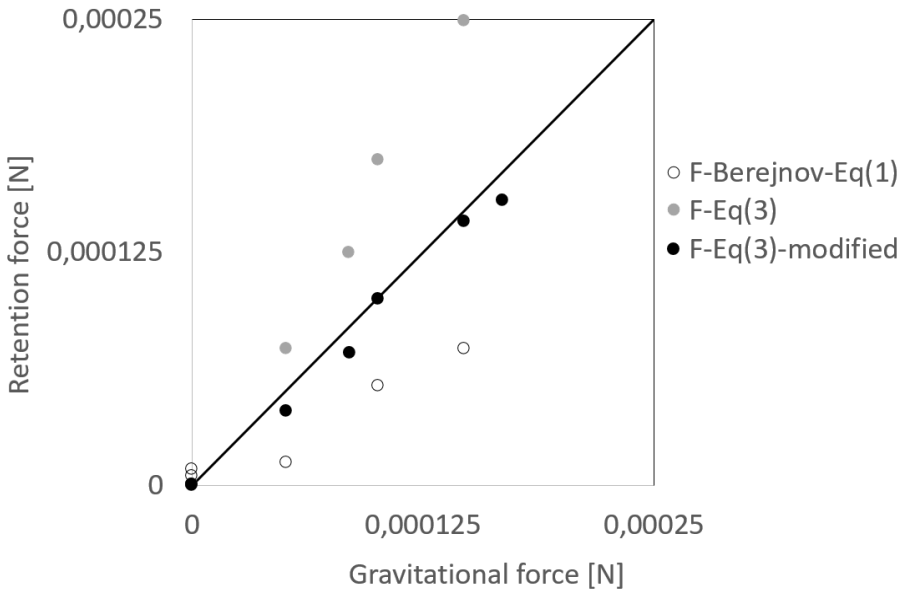

Fig. 6. Retention force vs. gravitational force for 30 µl and 50 µl droplets.

When comparing our data to those of Berejnov [8], the force range in our experiments corresponds to regimes of droplet deformation, but still static. The transition to the dynamic regime occurs for 30µl droplets at around 0.2 mN and for 50 µl droplets at 0.23 mN. However, we do not cover dynamic droplet behavior in these experiments.

3.2 Experimental results for fluorescence analysis

Generally, we use the fluorescence analysis for liquid film thickness measurements. The film thickness gradient near the contact line correlates with the contact angle if the contact angle is well below 90°. Johnson et al. [28] report contact angles of 20° as limit. Fluorescence signals remain undisturbed if the

apparent contact angle stays below this value. This hypothesis corresponds to configurations where the free liquid surface is almost parallel to the substrate. In practice, Johnson et al. [28] used prisms of fluorescent liquid with a constant inclination to evaluate this effect. In reality, the advancing front of a sliding droplet or rivulet clearly has a significant curvature.

So, the question arises: How does the fluorescence intensity change for contact angles, which are significantly larger than 20°? What happens if they become even larger than 90°? To answer these questions, we measured the fluorescence intensity for droplets in different states. We started with symmetrical droplets at rest on a horizontal plate and ended with strongly deformed droplets on an inclined plate. The apparent contact angles strongly differed at the advancing and receding sides. In extreme cases, droplets ran off the plate. However, our interest was on static droplets with large contact angle difference between front and back.

As before, we generated 30 and 50 µl droplets on a horizontal plate and continuously tilted that plate until the droplets eventually left it. Again, two cameras captured that process, providing a shadow side-view image and a fluorescence top-view image.

The plots in Figure 7 show the resulting apparent advancing and receding contact angles for 30 and 50 µl droplets as function of Bo, which is a measure of the plate inclination. Both contact angles are equal at the beginning and continuously diverge with increasing Bond number. The apparent contact angle at the advancing side (black curve) increases, while it decreases for the receding part (blue curve). Additionally, there is an increasing scattering, first for the advancing side later for the receding side as well. This scattering is related to the beginning motion of the droplet. Berejnov [8] investigated this instability in detail, usually seen as slip-stop movements. Eventually, the droplets slide down the inclined plate within a fraction of a second.

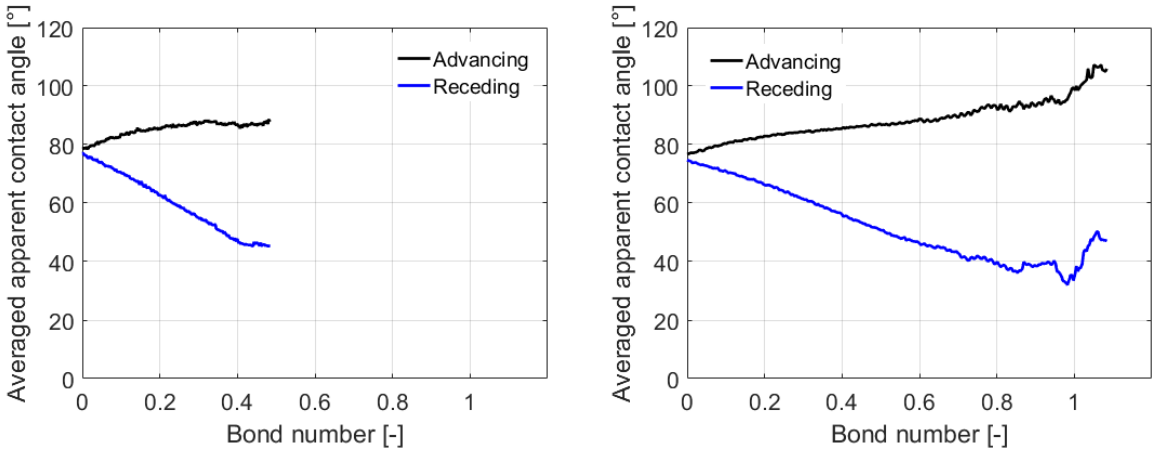

Fig. 7. Averaged apparent contact angle values for 30 µl (left) and 50 µl (right) droplets as function of Bo number. The black and blue curves correspond to the advancing and receding side, respectively.

Now, it is interesting to see the effect of changing surface curvature on the fluorescence signal. So, first the variation of surface curvature at the contact point of a single droplet during the inclination process of the plate is investigated (see Figure 8).

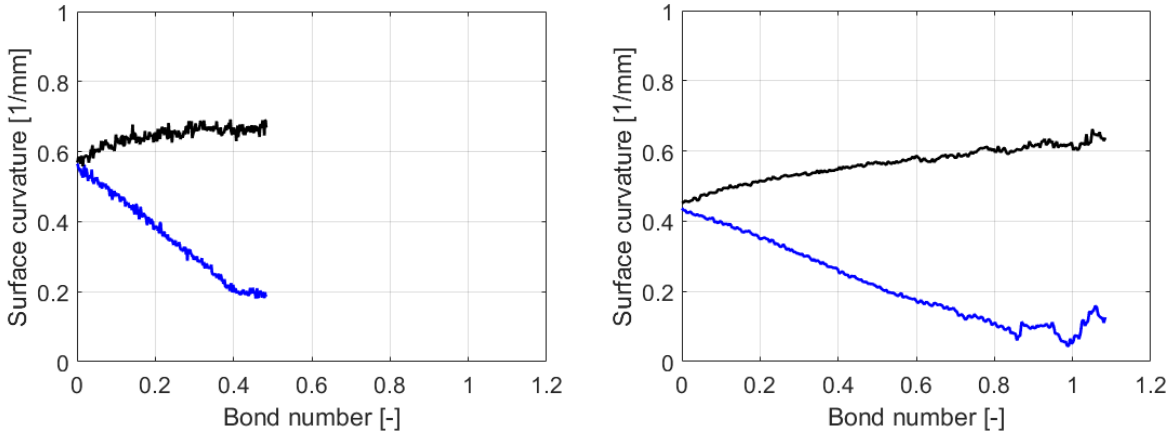

Fig. 8. Surface curvature at the contact point of single droplets at 30 µl (left) and 50 µl (right) as function of Bo number. The black and blue curves correspond to the advancing and receding side, respectively.

The advancing side curvature (black curve) does not undergo significant change, while the receding side curvature continuously decreases. This means that the receding side of the droplet becomes more and more flat. This is comparable to the test case of Johnson et al. [28], where they used fluorescent liquid prisms. As a consequence, the most accurate fluorescence signal with respect to liquid film thickness measurements, comes from this droplet area.

Now, we evaluate the overall change of the fluorescence signal with a change of surface curvature. A calibration factor in mm/counts represents the fluorescence intensity. It relates the corresponding fluorescence or pixel intensity to the real liquid film thickness, which we obtain from the shadow images. Every single data point in the plots of Figure 9 corresponds to the slope value of a calibration curve, as shown in Figure 3. If tracing this in function of the corresponding surface curvature at that same point, one can observe in Figure 9, that the slope of the calibration function changes for a single droplet on a continuously tilted plate according to the droplet deformation.

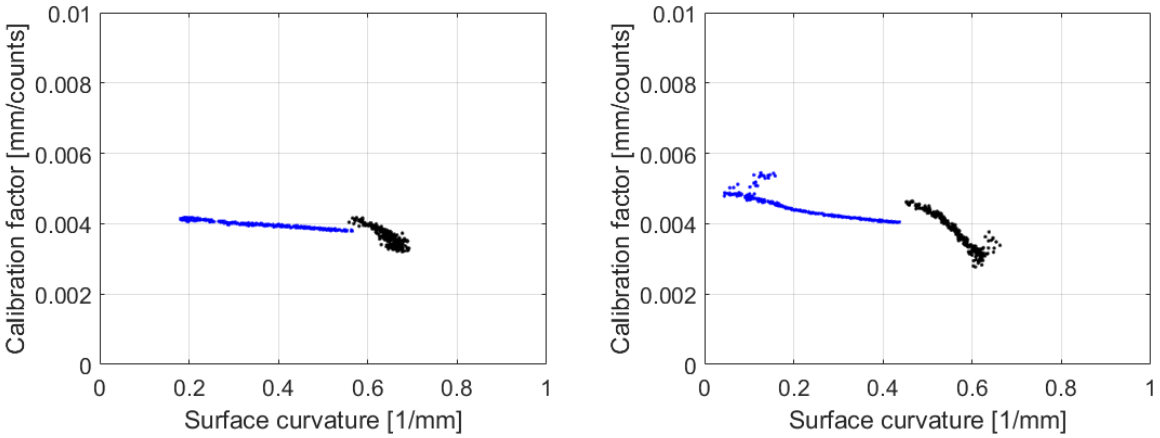

Fig. 9. Fluorescence calibration factor as function of the free surface curvature at the contact point. The black and blue curves correspond to the advancing and receding side, respectively.

Interestingly, the receding side of the droplet does not show significant variation of the calibration factor. It stays relatively constant, even for the large variation of the surface curvature. The outliers in

the right plot result from inflection of the rear droplet side. We do not consider them any further, as our focus is on droplets in static conditions. In contrast, the calibration factor strongly decreases for the advancing side of the droplet, where the surface curvature increases only half as much as it decreases for the receding side.

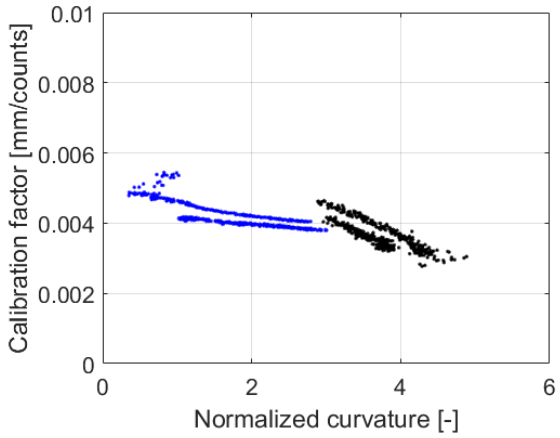

Fig. 10. Fluorescence signal modulation as function of the free surface curvature at the contact point. The black and blue curves correspond to the advancing and receding side, respectively. The lower and upper data points are from 30 and 50 µl, respectively.

Comparing the left and right plots of Figure 9, there is different curve progression for 30 and 50 µl droplets, including different transition points. Hence, the observed phenomenon is size-dependent. To exclude this dependency, we normalized the surface curvature with the total length of the droplets (see Figure 10).

An offset between both data sets remains, which could not be avoided. Hence, further experiments with more droplet volumes and different fluorescence setups are required to clarify this discrepancy. Nevertheless, new information was obtained concerning the applicability of fluorescence imaging to droplets and rivulets, as summarized next.

4 Conclusions

Two main aspects have been considered in this paper. The first part investigated the three-dimensional shape analysis of droplets on an inclined plate. Combining information from several shadow profiles with droplet perimeter, we derived the retention force for water on a painted metal plate. A modification is required in order to match retention force and gravitational force. Eventually, this leads to a new retention force factor of k=1.84, which involves the advancing and receding fronts together with half of the droplet perimeter. This value is the same for all our cases, without any further assumption on the shape of the droplets.

In a second experimental part, we investigated the effect of liquid shape on the fluorescence signal. Some issues remain. However, important questions have been solved regarding applicability and limitations of the fluorescence imaging method for film thickness measurements. The calibration procedure for fluorescence imaging contains more complex dependencies than generally assumed. Even if it is possible to keep all fluorescence parameters (dye concentration, illumination intensity, and temperature) constant and homogenously distributed within the liquid, the fluorescence signal strongly depends on the liquid shape. Highest deviations are observed for a larger surface curvature, particularly near the contact line. This is unfortunately where the situation is most interesting.

Contradicting our expectations, the deviation is not only found for situations involving contact angles larger than 90°. It is found that a certain curvature threshold already triggers this effect. The conversion of fluorescence intensity to film thickness seems reliable and almost constant below this curvature threshold. When exceeding this value, the calibration factor changes strongly and the measurement error increases. A correction of the fluorescence signal is not possible without additional information. Future experiments are needed with other droplet volumes and different fluorescence setups (dye tracer, illumination system).

Acknowledgment

The authors would like to thank Tim Lüft who supported the experiments described in this paper.

References

[1] Hagemeier, T., Thévenin, D. and Zähringer, K.: Stereoscopic fluorescence analysis of films, droplets and rivulets. In: 16th International Symposium on Applications of Laser Techniques to Fluid Mechanics, Lisbon, Portugal, 282/1-282/8, 2012

[2] Hagemeier, T., Bórdas, R., Zähringer, K., Thévenin, D.: Two-perspective fluorescence analysis of droplets creeping down a tilted plate. Exp. Fluids, 55-1639, 2014

[3] Schulz, F., Schmidt, J. and Beyrau, F.: Development of a sensitive experimental set-up for LIF fuel wall film measurements in a pressure vessel. Exp. Fluids, 56:98, 2015

[4] ElSherbini, A.I. and Jacobi, A.M.: Liquid drops on vertical and inclined surfaces I. An experimental study of drop geometry. J. Colloid Interface Sci., 273, 2004

[5] ElSherbini, A.I. and Jacobi, A.M.: Liquid drops on vertical and inclined surfaces II. A method for approximating droplet shapes, J. Colloid Interface Sci., 273, 2004

[6] Annapragada, S. R., Murthy, J. Y., Garimella, S. V.: Droplet retention on an incline. Int. J. Heat Mass Transfer 55 (5-6), 1457-1465, 2012

[7] Annapragada, S. R., Murthy, J. Y., Garimella, S. V.: Prediction of droplet dynamics on an incline. Int. J. Heat Mass Transfer 55 (5-6), 1466-1474, 2012

[8] Berejnov, V., Thorne, R.: Effect of transient pinning on stability of drops sitting on an inclined plane. Phys. Rev. E 75, 066308, 2007

[9] Decker, E., Frank, B., Suo, Y., Garoff, S.: Physics of contact angle measurement. Colloids Surf., A 156, 177-189, 1999

[10] Eggers, J.: Toward a description of contact line motion at higher capillary numbers. Phys. Fluids 16, 3491-3494, 2004

[11] Fan, J., Wilson, M., Kapur, N.: Displacement of liquid droplets on a surface by a shearing air flow. J. Colloid Interface Sci. 356, 286-292, 2011

[12] Frenkel, Y. I.: Rolling of a drop on an inclined plane. Zh. Eksp. Teor. Fiz 18 (7), 659-667, 1948

[13] Greszik, D., Yang, H., Dreier, T., Schulz, C.: Measurement of water film thickness by laser-induced fluorescence and Raman imaging. Appl. Phys. B 102, 123-132, 2011

[14] Kwok, D., Neumann, A.: Contact angle measurement and contact angle interpretation. Adv. Colloid Interface Sci. 81 (3), 167-249, 1999

[15] Le Grand, N., Daerr, A., Limat, L.: Shape and motion of drops sliding down an inclined plane. J. Fluid Mech. 541, 293-315, 2005

[16] Lehwald, A., Thévenin, D., Zähringer, K.: Quantifying macro-mixing and micro-mixing in a static mixer using two-tracer laser-induced fluorescence. Exp. Fluids 48, 823-836, 2010

[17] Macdougall, G., Ockrent, C.: Surface energy relations in liquid/solid systems. i. the adhesion of liquids to solids and a new method of determining the surface tension of liquids. Proc R Soc A180, 151-173, 1942

[18] Pepin, X., Blanchon, S., Couarraze, G.: Powder dynamic contact angle measurements: Young contact angles and effectively wet perimeters. Powder Technol. 99 (3), 264-271, 1998

[19] Pierce, E., Carmona, F., Amirfazli, A.: Understanding of sliding and contact angle results in tilted plate experiments. Colloids Surf., A 323 (1-3), 73-82, 2008

[20] Podgorski, T., Flesselles, J.-M., Limat, L.: Corners, cusps, and pearls in running drops. Phys. Rev. Lett. 87, 036102, 2001

[21] Rio, E., Daerr, A., Andreotti, B., Limat, L.: Boundary conditions in the vicinity of a dynamic contact line: Experimental investigation of viscous drops sliding down an inclined plane. Phys. Rev. Lett. 94 (2), 024503, 2005

[22] Šikalo, Š., Wilhelm, H.-D., Roisman, I., Jakirlić, S., Tropea, C.: Dynamic contact angle of spreading droplets:

Experiments and simulations. Phys. Fluids 17, 062103, 2005
[23] Snoeijer, J., Andreotti, B.: Moving contact lines: scales, regimes and dynamical transitions. Annu. Rev. Fluid Mech. 45, 269-292, 2013
[24] Snoeijer, J., Peters, I., Limat, L., Daerr, A.: Simple views on cornered contact lines near instability. In: Proceedings of the 23rd CANCAM. pp. 172-174, 2011
[25] Štěpánek, F., Ansari, M.: Computer simulation of granule microstructure formation. Chem. Eng. Sci. 60 (14), 4019-4029, 2005
[26] Hagemeier, T., Hartmann, M., Thévenin, D.: Practice of vehicle soiling investigations: A review. Int. J. Multiphase Flow 37 (8), 860-875, 2011
[27] ElSherbini, A.I., Jacobi, A.M.: Retention forces and contact angles for critical liquid drops on non-horizontal surfaces. J. Colloid Interface Sci. 299, 2006
[28] Johnson, M.F.G., Schluter, R.A., Bankoff, S.G.: Fluorescent imaging system for global measurement of liquid film thickness and dynamic contact angle in free surface flows. Rev. Sci. Instrum. 68 (11), 1997

Copyright Statement